Acta Oceanol. Sin., 2019, Vol. 38, No. 3, P. 26–35
https://doi.org/10.1007/s13131-019-1396-4
http://www.hyxb.org.cn
E-mail: hyxbe@263.net

The influence of runoff and wind on the dispersion patterns of suspended sediment in the Zhujiang (Pearl) River Estuary based on MODIS data

Suying Ou[1, 2], Qingshu Yang[1, 2], Xiangxin Luo[1, 2*], Fan Zhu[1], Kaiwen Luo[1], Hao Yang[1]

[1] Institute of Estuarine and Coastal Research, School of Marine Sciences, Sun Yat-sen University, Guangzhou 510275, China

[2] State-province Joint Engineering Laboratory of Estuarine Hydraulic Technology, Guangzhou 510275, China

Received 23 November 2017; accepted 27 February 2018

Abstract

Cloud-free moderate-resolution imaging spectroradiometer (MODIS) images of the Zhujiang (Pearl) River Estuary (ZRE) taken between 2002 and 2012 are retrieved and used to study the spatial and temporal patterns of suspended sediment concentrations (SSCs) across the estuary under runoff, wind, and tropical storm conditions. Five typical dispersal patterns of suspended sediments in the estuary are defined: Case I shows generally low SSCs under low dynamics; Case II shows a river-dominant dispersal pattern of suspended sediments from the outlets, particularly from Modaomen, Jiaomen, Hengmen, and others; Case III shows wind-dominant dispersal of high SSCs derived from the west shoal and southwesterly transport under a strong NE wind; Case IV is the combination of relatively large runoff and wind; and Case V is caused by a strong tropical storm with high river discharge and wind, which is characterized by the high SSCs across the entire estuary that are transported eastward by wind-driven and buoyancy currents outside the estuary. Runoff is a dominant factor that controls seasonal and annual SSC variations in the ZRE, with the area of high SSCs being largest in the summer and smallest in the spring. The correlation coefficients between the monthly averaged river-suspended sediment discharge and the area of the high SSCs are approximately 0.6. The wind power over the west shoal increases with a wind speed, which induces more sediment resuspension and shows a close relationship between the wind speed and high SSC area.

Key words: Zhujiang (Pearl) River Estuary, suspended sediment concentration (SSC), moderate-resolution imaging spectroradiometer, wind, runoff, tides

Citation: Ou Suying, Yang Qingshu, Luo Xiangxin, Zhu Fan, Luo Kaiwen, Yang Hao. 2019. The influence of runoff and wind on the dispersion patterns of suspended sediment in the Zhujiang (Pearl) River Estuary based on MODIS data. Acta Oceanologica Sinica, 38(3): 26–35, doi: 10.1007/s13131-019-1396-4

1 Introduction

The suspended sediment concentration (SSC) plays an important role in estuarine geomorphology, water quality, and ecology. The SSC influences the evolution of estuarine morphology (Cuvilliez et al., 2015), alters light attenuation (Lawson et al., 2007), and affects the cycles of nutrients, organic micro-pollutants, and heavy metals (Percuoco et al., 2015; Fagherazzi et al., 2014). An understanding of suspended sediment dynamics is essential to investigate the quantification of fluxes of ecologically and chemically important substances and determine the fate of pollutants in estuarine environments (Chen et al., 2015; Li et al., 2012).

Because the estuaries are transition zones between land and sea, sedimentary processes, such as flocculation, deposition, transport and erosion, are influenced by factors such as fluvial runoff, tides, mixing, winds, and waves (Liu and Huang, 2012; Gong and Shen, 2012). The multi-scale changes in these driving forces affect sediment dynamics and result in the complex spatio-temporal distribution of suspended sediments in the estuaries (Petus et al., 2014). Sediment resuspension and transport controlled by tidal currents cause SSC levels to follow the tidal cycle (Li et al., 2015), and temporal variations in the SSC are at intratidal to annual timescales. Responses to river discharge and sediment load have been examined in previous studies (Liu and Wang, 2014). Other factors, such as wind-induced mixing and waves and especially storm events, can also cause the variations in SSC levels (Bourrin et al., 2008; Fernández-Nóvoa et al., 2015; Freeman et al., 2015; Green and Coco, 2014; Chen et al., 2012).

Because of the large number of driving factors, including storms, discharge rate, tidal cycles, the magnitude and direction of wind stress, bathymetry, and topography, it is difficult to generalize the spatial and long-term characteristics of total suspended sediment concentration (Lahet and Stramski, 2010). Traditional measurement methods, such as shipboard surveys or mooring arrays, are insufficient to study the SSC variability. In recent years, an ocean color remote sensing technology has been developed, and satellite images, such as moderate-resolution imaging spectroradiometer (MODIS) data, have been successfully used to monitor the SSC variability in lakes and estuaries at high spatial and temporal resolutions (Lihan et al., 2008; Doxaran et al., 2012; Nezlin et al., 2008; Moreira et al., 2013; Wu et al., 2014; Feng et al., 2014; Petus et al., 2010).

Foundation item: The National Natural Science Foundation of China under contract Nos 41106015 and 41476073; the National Key Research and Development Program of China under contract No. 2016YFC0402600.
*Corresponding author, E-mail: Luoxx6@mail.sysu.edu.cn

The Zhujian (Pearl) River Estuary (ZRE) at the northeastern end of the South China Sea receives 3.26×10^{11} m^3/a of fresh water and 88.7 Mt/a of sediment from the Zhujiang (Pearl) River. The South Asian monsoon causes well-defined seasonal changes in the Zhujiang River from the wet to the dry seasons, and the wind regime across the ZRE also changes seasonally. The effects of tides, runoff, and monsoon winds on the intra-tidal to annual changes in the ZRE plume have been previously studied (Ou et al., 2009; Zu et al., 2014). However, several questions remain: How do the spatial characteristics of the SSC change in the ZRE under the complex influence of topography, runoff, tides and wind? In particular, how do the multiple sources of runoff affect the spatial characteristics of the SSCs in the ZRE? How is sediment processing in the ZRE affected by the tropical storms that frequently enter the ZRE during the wet season? A complete perspective and understanding of the distributions of SSCs throughout the ZRE is still lacking. In this study, cloud-free high-resolution spatial and temporal MODIS images of the ZRE for the period from 2002 to 2012 were used. The SSCs were derived from the MODIS images using an empirical formula that we previously developed, and the retrieved spatial distributions of the SSCs were analyzed. The correlations between runoff rates and wind with the horizontal dispersal pattern were studied, and their influences on the SSC are discussed.

2 Data and methods

2.1 *Situ data*

As one of the large-scale estuary systems in the world, the ZRE has a complicated topography composed of three main bays (Lingding, Modaomen and Huangmao) with multiple sources of sediment input from eight outlets of the Zhujiang River Delta. As shown in Fig. 1, as one of the large-scale estuary systems in the world, the Yamen (YM) and Hutiaomen (HTM) outlets drain into Huangmao Bay; the Jitimen (JTM) and Modaomen (MDM) outlets drain into the Modaomen Estuary; and to the east, the Hengmen (HEM), Hongqili (HQL), Jiaomen (JM), and Humen (HM) outlets drain into the Lingding Bay and form three shoals with two channels. Data for spring and neap tides in the Lingding Bay were collected by four surveys. The observation stations are marked with different symbols in Fig. 2. The first survey of 20 stations was performed on 19–21 and 25–26 June 2002, and a survey of 12 stations was conducted during 1–2 and 4–5 July 2002 near the west Lingding Bay. In the west shoal of Lingding Bay, simultaneous observations at seven stations during 6–7 July 2005 were used. In these three surveys, the velocity and salinity were measured, 500 mL water samples were collected hourly at every station at 6 layers from the surface to the bottom, and the SSCs were estimated in the laboratory by filtering and weighing the water samples. Additionally, hourly water samples at five stations from the surface, middle and bottom layers were collected on 13 and 14 August 2007, and the SSCs were measured to match the satellite data.

2.2 *MODIS data*

MODIS data (Bands 1 and 2 with a resolution of 250 m, and Bands 3–7 with a resolution of 500 m) were obtained from the NASA website data center (http://ladsweb.nascom.nasa.gov/data/search.html). The MODIS data were pretreated using remote sensing image processing software ENVI (environment for visualizing images). First, the image projection was converted to a UTM-WGS84 projection, the butterfly effect of satellite imaging was removed, and the image region (21°30′–23°00′N, 111°50′–115°10′E) of the ZRE was clipped. An ENVI FLAASH model was then used to carry out atmospheric correction to eliminate the errors caused by atmospheric effects, and ENVI masking tools were used to cover the land area and cloud cover; the true reflectances of all the features on the ground were thus obtained.

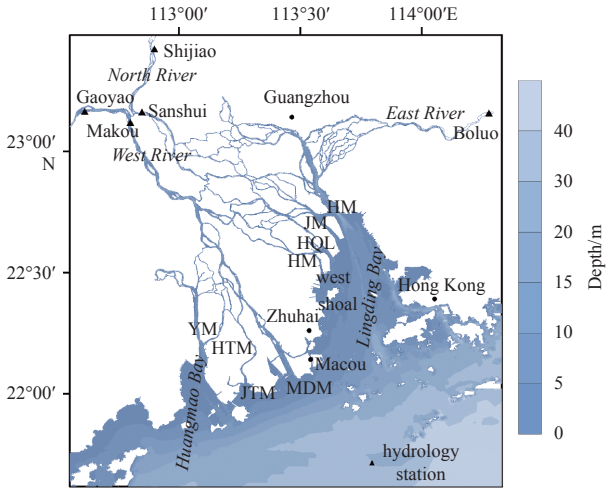

Fig. 1. Location and topography of the ZRE. The abbreviations refer to the rivers flowing into the estuary as follows: YM, Yamen; HTM, Hutiaomen; JTM, Jitimen; MDM, Modaomen; HEM, Hengmen; HQL, Hongqili; JM, Jiaomen, and HM, Humen.

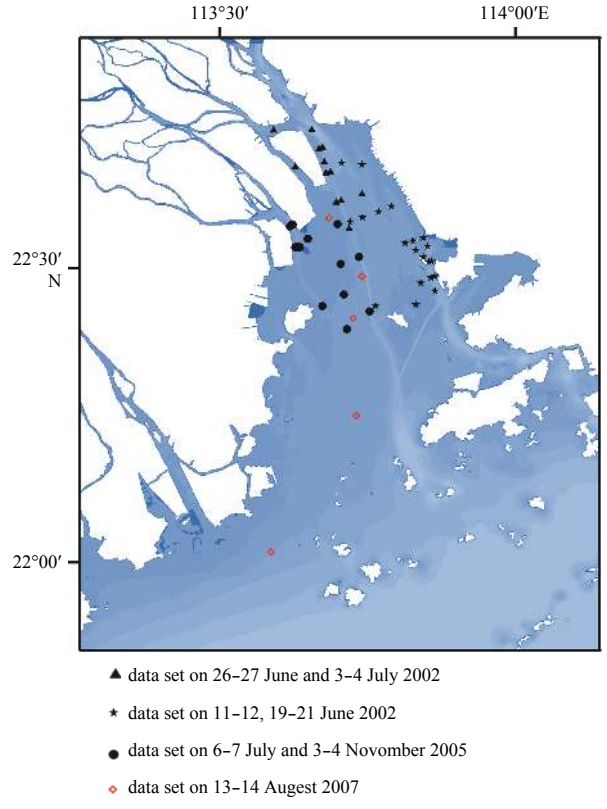

Fig. 2. The stations of the four surveys used to validate the MODIS retrieval formula.

2.3 *SSC retrieval*

There are two reflection peaks in the spectral curves that in-

dicated the SSCs in water obtained from the ZRE estuarine water; the main reflection peak was in the red wavelengths of Band 1, and the secondary peak was in the near infrared band of Band 4 (Xing et al., 2013). A strong correlation was demonstrated between the suspended sediment concentrations in the turbid estuary environment and MODIS Bands 1 or 4 and was integrated into empirical algorithms to quantify the concentrations of suspended matter or the turbidity levels in marine waters (Petus et al., 2010; Chen et al., 2011). Linear, exponential, logarithmic, parabolic and cubic relationships between the SSC and a water reflectance have been found in MODIS images and have been compared. Xing et al. (2013) developed an exponential regression model to estimate the SSC concentrations of Lingding Bay. Previous studies have demonstrated that MODIS Band 1 produces adequate remote sensing products for coastal waters (Nezlin et al., 2008; Feng et al., 2014). Despite some errors, an empirical retrieval relationship can still be used to study the variation in total suspended matter and the spatio-temporal variability in river plumes (Lahet and Stramski, 2010; Petus et al., 2014).

In this study, we also use the *in situ* SSC data of four surveys to fit the water reflectance and established empirical algorithms to retrieve the SSCs for the entire study area. From the *in situ* data, we found that the hourly changes in the SSC of the ZRE were significant and may have been caused by the tidal current. However, the MODIS imaging only represented the spatial distribution at one time in each day. To match the imaging time and the hourly *in situ* data, the specific field SSC data were selected if the time gaps between the acquisition of the MODIS imagery and field sampling were less than 30 min. The reflectance data at the field stations were interpolated to 250 m×250 m or 500 m×500 m grids. The non-linear regression relationship between the water reflectance of Bands 1–4 and the corresponding measured SSC was established and confirmed that an exponential retrieval algorithm between the SSC of the ZRE and Band 1 of the water reflectance was best; the correlation index (R^2) was up to 0.77 (Fig. 3). The regression also reveals a finely defined relationship between the water reflectance of Band 1 under cloud-free conditions and the SSC, and we thus use this algorithm to retrieve SSC data from the cloud-free MODIS images.

Cloudy and rainy days are common over the ZRE, with the frequency for Hong Kong and Zhuhai exceeding 85.0% each year. In this study, only 108 cloud-free MODIS images of the ZRE were obtained during the study period of 2002–2012, which were used to determine the annual SSC variability. After preprocessing and atmospheric correction by the ENVI software, the water reflectance of Band 1 is used to calculate the SSCs at a resolution of 250 m×

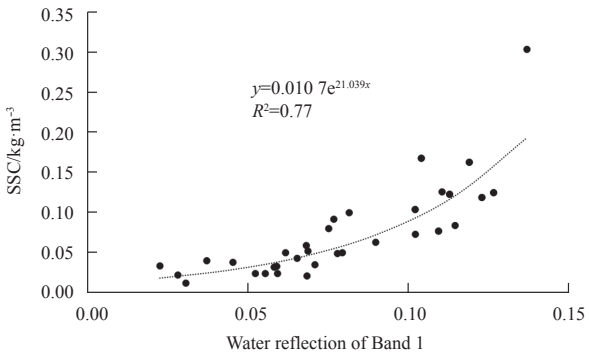

Fig. 3. Relationship between SSC and water reflectance from MODIS Band 1.

250 m using our exponential retrieval model (Fig. 3). The SSC horizontal distribution area covered by the ZRE (21.50°–22.75°N, 112.85°–114.00°E) of the 108 images was calculated with five SSC levels using the following criteria: very low concentrations (0.01 kg/m^3<SSC<0.05 kg/m^3), low concentrations (0.05 kg/m^3< SSC<0.1 kg/m^3), medium concentrations (0.1 kg/m^3<SSC< 0.15 kg/m^3), higher concentrations (0.15 kg/m^3<SSC<0.2 kg/m^3), and high concentrations (SSC>0.2 kg/m^3).

2.4 *River flow and wind data*

The monthly discharge and the sediment transport rates were calculated for the period of 2002–2012; data were collected from the tributaries at the Makou Hydrological Station (on the West River), from the Sanshui Hydrological Station (on the North River), and from the Boluo Hydrological Station (on the East River). Over this period, the West River accounted for approximately 70.0% of river runoff and 71.0% of the suspended sediment load carried by the Zhujiang River into the ZRE. The mean flow and sediment load at the Makou Station averaged over this period were 6 348 m^3/s and 721 kg/s, respectively, whereas at the Sanshui Station they were 1 767 m^3/s and 187 kg/s, respectively. The Zhujiang River flow and the sediment load follow a clear seasonal pattern, with increased discharge in summer and spring (May to August) and a significant reduction during the dry season (October to February) (Fig. 4). The maximum monthly discharge (>37 000 m^3/s) was observed in July, and the minimum occurred in January. The sediment load is the greatest between June and August at up to 10 000 kg/s; however, the monthly sediment load discharged into the ZRE during winter is very low, less than 80 kg/s. Months with a high mean river flow showed greater

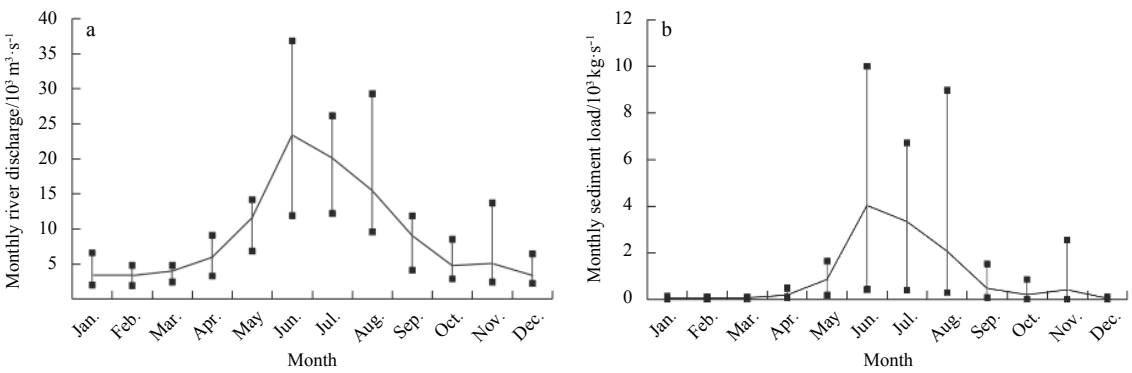

Fig. 4. Annual cycle of average monthly discharge (a) and monthly sediment load (b) for the Zhujiang River over the period of 2002–2012, showing the monthly average (solid black line) and minimum and maximum monthly values over this period.

variability because they coincided with localized periods of heavy rainfall and increased sediment supply that cause large variations around the long-term mean values (Fig. 4b).

Wind data were retrieved from the climate forecast system reanalysis (CFSR) database (http://rda.ucar.edu/pub/cfsr.html) developed by the NOAA's National Centers for Environmental Prediction (NCEP). The CFSR provides a spatial resolution of 0.5°×0.5° and a 6 h time resolution. This database has been successfully used in previous studies (Alvarez et al., 2014). Over the ZRE region between 21.5°–22.5°N and 113°–114°E, a statistical analysis was carried out on the wind data from six points. The wind over the ZRE is typically monsoon-dominated and has well-defined seasonal variability. An SW wind is dominant in summer and an NE wind in winter. During the period of 2002–2012, strong northeasterlies were dominant over the ZRE, with an occurrence frequency greater than 40.0%, followed by easterly and southwesterly winds (Fig. 5). Wind speeds greater than 20 m/s were all observed in summer during tropical typhoons, and the wind direction varied among SW, SE and NE. The stronger NE winds with a speed greater than 15 m/s were always observed during the period of winter cold air invasions. During the period of 2002–2012, the frequency of strong winds (>10 m/s) was approximately 14.0% and the frequency of light winds (<4 m/s) was approximately 20.0%.

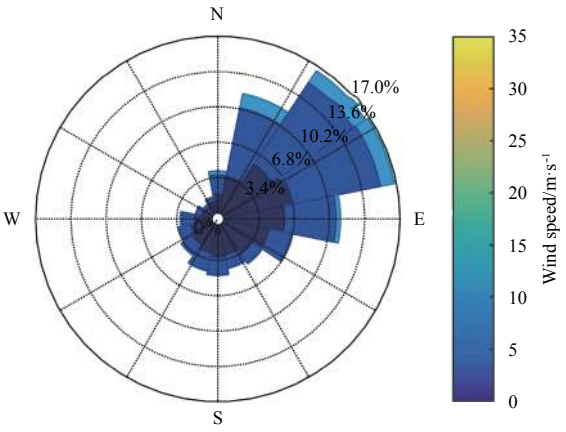

Fig. 5. Wind rose for the ZRE over the period of 2002–2012.

3 Results

The retrieved surface SSC distributions are the result of sediment movement during the study period. Suspended sediment from the Zhujiang River is transported into the estuary via the interaction of river discharge and tides. The combination of wind waves and the higher flood or ebb tidal velocity is responsible for the resuspension and transport of sediment. The sediment supplied by the Zhujiang River is redistributed across the Zhujiang River Delta and discharged into the ZRE through eight outlets, and the relative contribution of each outlet affects the spatial SSC pattern. Under extreme typhoon conditions, the pattern of SSC dispersal in the ZRE is more complex because of additional factors such as heavy rain, floods and strong winds. With respect to the complex sediment transport processes, especially the resuspension of bottom sediment and the transport of suspended sediments driven by different forcing factors, such as runoff, wind and tides that affect the ZRE, the surface SSC shows correspondingly complex horizontal distributions for all 108 images.

The surface SSC distributions at the time of imaging are the result of all driving force co-interactions in the estuary; however, at any one time, one or two forcing factors were dominant, which produced the corresponding horizontal distribution. The wind is weak in most field surveys (Fig. 2), and the dominant effects of tide and river discharge were considered. The tidal current is a periodic driver, except when a large ebb or flood current could have dominated suspended sediment transport and perhaps have caused a high SSC in a spring tide. However, at a low ebb or flood current during a spring tide or a neap tide, the tide could not have caused a high SSC in water and there must have been another driving force, such as a river discharge or salt wedge, which overlapped the tide's effect to dominate the surface distribution of the high SSC. In the flood season, with large fresh water and sediment inputs into the estuary, the maximum surface SSC and average tidal SSC are larger than in the dry season, which has a low river discharge and sediment load. Therefore, in a flood season with a low tidal current, the river discharge is an important dominant factor that affected the high SSC distribution in the estuary. However, in a dry season with no wind effect, the tidal current is the dominant driver of SSC distribution, and the SSC is low for most of the day. When the wind increases, the wind-induced waves and currents may co-act on the SSC with the tides and the river discharge.

To link the SSC surface distribution to the dominant driving force, the tide, river discharge and wind at the imaging time were first estimated. The tide at the imaging time was simulated using the Oregon State University Tidal Prediction Software (OTPS, http://volkov.oce.orst.edu/tides), and the average of the Zhujiang River discharge data for 3 d and the wind data that affected the ZRE before the imaging time of all images were considered. By comparing the relative strengths of the wind, tide, and river discharge linked to the SSC distribution, we find some typical or special suspended sediment distributions induced by a dominant river or wind forcing which overlapped or combined with the tidal effect; five typical spatial dispersal patterns of suspended sediment were defined and are outlined below. However, if this could not distinguish the dominant driving force of the SSC dispersion and the horizontal SSC distribution variation was more complex, such as in Case 4, those horizontal distributions were not outlined.

3.1 *Case I: low SSC under weak wind and low runoff*

Under good weather with weak winds (3 d average speed less than 4.0 m/s) and less runoff from the Zhujiang River, the SSC distribution was between 0.02 and 0.06 kg/m^3 across the ZRE, as shown in Fig. 6, with only the SSC of the shoals adjacent to the coast or near the eight outlets being close to 0.06 kg/m^3. In this condition (Fig. 6), the wind is weak, the 3 d average of the Zhujiang River discharge is less than 3 000 m^3/s, and the tide in the ZRE at the imaging date is a neap tide, as shown in Table 1. The ZRE is under low dynamics, the suspended sediment from the Zhujiang River is very low (approximately 15.0 kg/s), and the neap tidal current is lower than the flood current. Most of the time, the neap tidal current could not resuspend the ZRE fine bottom sediments and the SSC in the ZRE is thus low. This case was always observed in the neap tides of late autumn and in winter under low runoff and weak wind conditions.

3.2 *Case II: river-dominated dispersal pattern of suspended sediment*

Under a high river discharge and a suspended load from the Zhujiang River but in good weather with a weak wind, we could observe large suspended sediment loads from the Zhujiang River Delta coming into the ZRE, as shown in Fig. 7. In this case, the 3 d

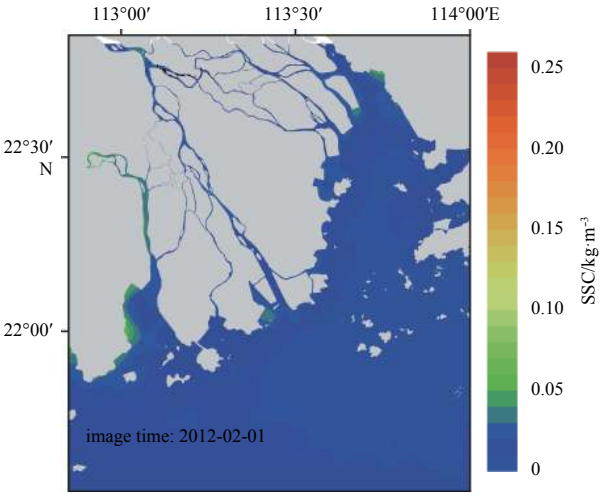

Fig. 6. MODIS-derived horizontal SSC distribution under low runoff and a weak wind.

average of the Zhujiang River discharge is greater than 30 000 m^3/s, and the suspended sediment discharged into the estuary is approximately 18 000–23 000 kg/s, as shown in Table 1. Under a huge runoff into the ZRE, high SSC levels spread from the tributary mouths and move into the adjacent estuarine waters, whereas the SSCs of the other shoals were low, as shown in Fig. 7. In Fig. 7, the ZRE is under a weak SW–WSW wind, either a spring tide or a neap tide, the suspended sediment is derived from the eight outlets, and the greater the amount of sediment supplied by the outlets, the higher the offshore SSC and the greater the high-SSC area. Therefore, in this condition, the suspended sediment dispersal is controlled by a large runoff and its related residual current.

The most prominent characteristic of this dispersal pattern is the higher SSC (>0.2 kg/m^3) over the MDM outer shoal and west shoal of the Lingding Bay adjacent to the mouths of the MDM, HM, HQL and JM outlets. For the Zhujiang River Delta, the eight distributaries (Fig. 1) control the levels of discharge and sediment supply from the Zhujiang River into the different parts of the three subestuaries. The Modaomen is the main outlet and supplies approximately 25.0% of the Zhujiang River's discharge and 36% of the suspended sediment load. Approximately 40.0% of the Zhujiang River's total discharge and suspended sediment load pass through the Hengmen, Hongqimen, and Jiaomen outlets into the west shoal of Lingding Bay. As shown in Fig. 7b, during the flood season, when the Zhujiang River discharge exceeds 30 000 m^3/s, this redistribution by the eight outlets cause a spatial pattern in which the SSCs were higher over the MDM and the west shoal of the Lingding Bay than near the other outlet shoals and is the dominant factor in the development of these spatial SSC distributions.

3.3 *Case III: NE wind-dominated resuspension and dispersal pattern of suspended sediment*

Wind affects the SSCs of a water column through the processes of fine sediment resuspension and transport. Wind-driven sediment resuspension is the result of the transfer of momentum into the water layers and the formation of wind waves that disturb the sediment bed. This leads to the resuspension of fine bed sediments by wind-driven waves in shallow nearshore zones and an increase in the SSC levels. Moreover, the net suspended sediment transport is directly influenced by the wind-driven currents.

Table 1. Dynamic statistics during or before MODIS imaging time

Case	Imaging date	Zhujiang River		Wind		Tide	
		$Q/m^3 \cdot s^{-1}$	$Q_s/kg \cdot s^{-1}$	$W/m \cdot s^{-1}$	Direction	H/m	Type
I	2012–02–01	2 365	15.6	3.6	NNE	0.49	neap
II	2009–07–09	38 223	22 370.0	4.0	SSE	1.41	spring
	2002–07–05	32 505	18 154.0	3.2	SW	0.67	neap
III	2003–12–14	4 220	102.0	8.7	NE	0.90	medium
IV	2003–08–03	12 394	2 024.0	4.4	WSW	1.08	medium
V	2008–06–20	55 484	47 154.0	6.4	SSW	1.18	spring

Note: Q and Q_s are the 3 d averaged Zhujiang River and suspended sediment discharges, respectively; W is the 3 d averaged wind speed; and H is the tidal range.

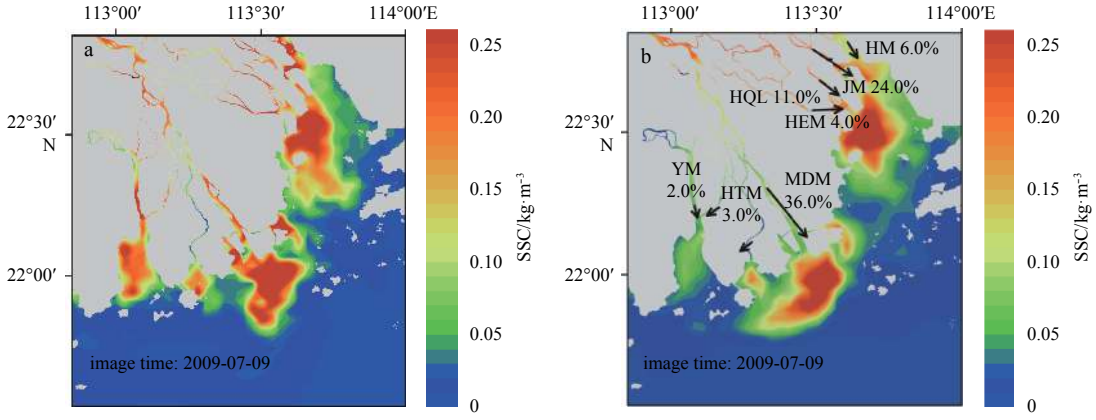

Fig. 7. MODIS-derived horizontal SSC distribution for 9 July 2009 (a) and 5 July 2002 (b) under large runoff and weak wind. Figure 7b is the proportion of suspended sediment input to the ZRE supplied by each of the eight outlets.

As shown in Fig. 8, when the wind over the ZRE is strong, the dispersal pattern of suspended sediment is very different from the river-dominant type. The MODIS imaging reveals a high SSC between 0.08 and 0.15 kg/m^3 that spread southwest along the west shoal and outer shoals, as shown in Fig. 8. In this case, the high SSC levels from the outlets are not dominant or even very small; the three-day averages of the Zhujiang River discharge and suspended sediment load are approximately 4 500 m^3/s and 102 kg/s; however, the 3 d average wind speeds are more than 8.7 m/s, as shown in Table 1. Although the Lingding Bay is a semi-closed bay with small waves because of the shading effect of many islands in the outer estuary, relatively large wind waves are formed under the continuous strong wind (Yang and Chen, 1987). In the ZRE, the shapes of the Lingding and Huangmao Bays control the wind fetch and thereby influence the formation of wind waves. The fetch varies with the wind direction, which leads to spatial variations in a wave power. From 2002 to 2012, the NE wind was dominant (Fig. 5). Under the NE wind, the fetch along the eastern nearshore zone of the ZRE estuary is short, and the wind-wave influence is minor. However, the fetch along the western nearshore zone, especially over the southwestern shoals such as the Zhuhai west shoal, is longer and facilitates the formation of more powerful waves.

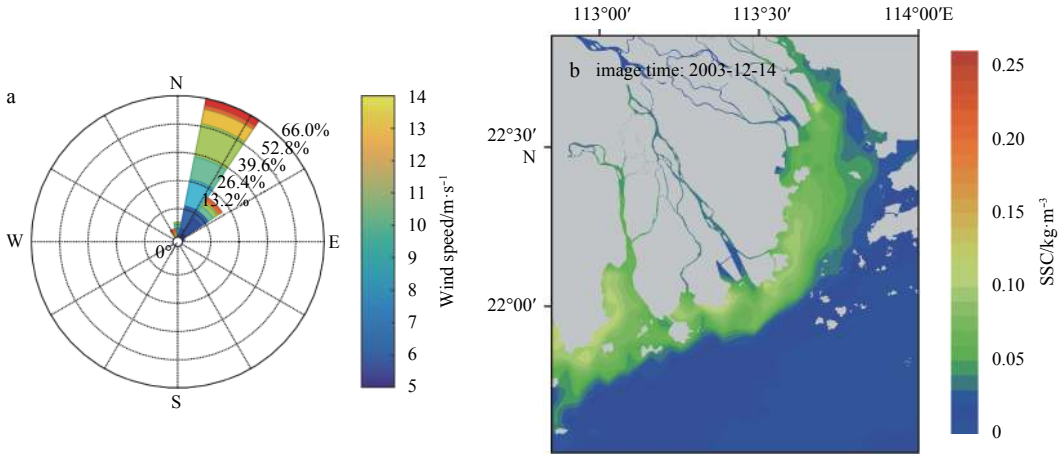

Fig. 8. Northerly wind rose (a) covering the 3 d prior to the date of the image in (b), and the resulting SSC dispersal in the ZRE under the NE wind (b).

The response of fine sediments to the continuous strong NE winds in the ZRE, i.e., the fine sediments in the shallow west shoal, is their re-suspension into the water column by the wind waves, and the high SSC levels are transported to the southwest by the southwestern wind-induced current via the buoyancy current (Fig. 8).

3.4 *Case IV: wind and river-induced dispersal pattern of suspended sediment*

In many cases, the sediment in the estuarine waters supplied by the outlets is more than that in winter but less than that in a flood event, as shown in Table 1. The Zhujiang River discharge is 12 000 m^3/s, and the suspended load into the estuary is approximately 2 000 kg/s, which is larger than the annual average runoff, and the SSC near the outlets is thus higher (Fig. 9). Moreover, under the relatively strong wind, fine sediment resuspended from the shoal beds caused a relatively high SSC between 0.05 and 0.15 kg/m^3 in the shallow shoal. Therefore, under the interaction of wind and runoff, the horizontal distribution of the surface SSC (Fig. 9) is more complex than the river-dominant (Fig. 7) and wind-dominant types (Fig. 8).

3.5 *Case V: Typhoon-dominant dispersal pattern*

The extreme condition, which develops under the typhoon conditions of strong winds and heavy rain across the ZRE, shows high SSC levels across the entire estuary and an SSC greater than 0.2 kg/m^3 in the outer estuary that spreads eastward, as shown in Fig. 10.

From May to October each year, tropical storms (typhoons) from the South China Sea and the western Pacific pass through or make landfall near the ZRE, and the associated strong winds and heavy rain in the ZRE lead to increases in the discharged and suspended sediment loads entering the ZRE. These complex and extreme driving forces affect the sources and transport of suspended sediment in the ZRE and resulted in the unusual dispersal of suspended sediment seen in Fig. 10. Between 18 and 27 June 2008, Typhoon Fengshen formed and gradually impacted the ZRE. The hourly Zhujiang River discharge (sum of the Gaoyao,

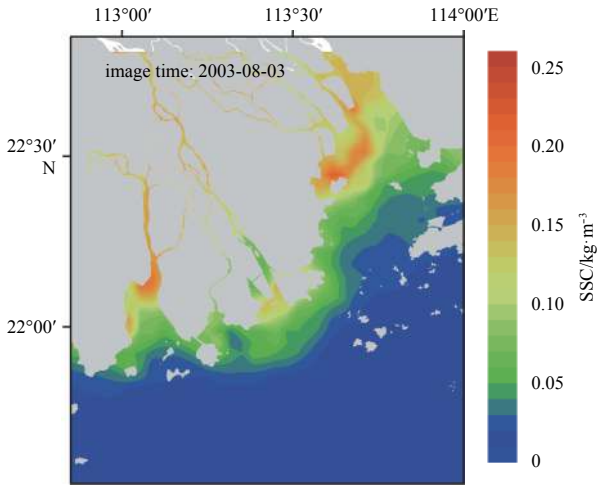

Fig. 9. The MODIS-derived horizontal SSC distribution under large runoff and wind.

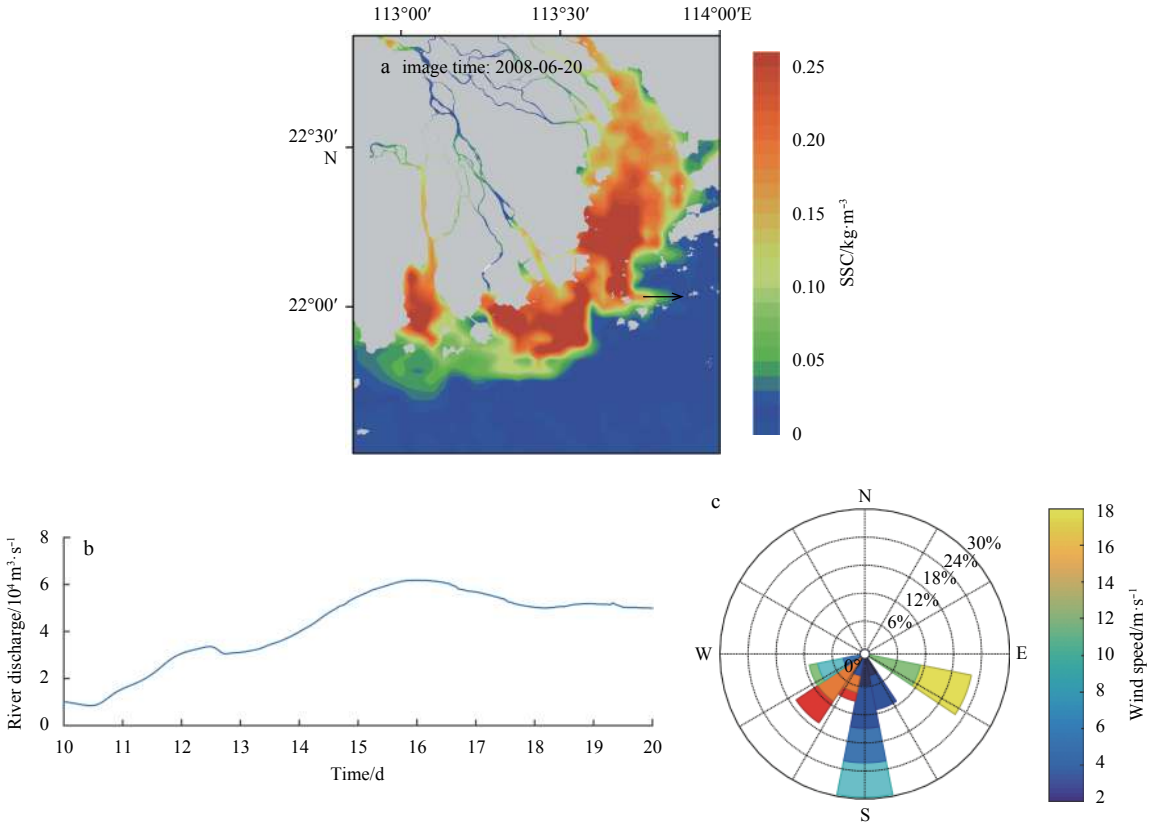

Fig. 10. MODIS-derived SSC dispersal (a) after tropical storm Fengshen generated increased Zhujiang River discharge (b) and strong winds (c). Figure 10b is variation in the Zhujiang River discharge over the 10 d prior to the date when the image. Figure 10c is the wind rose for the period of 12–20 June 2008. Arrow in Fig. 10a represents eastward flow caused by the SW wind and the buoyancy current.

Shijiao, and Boluo discharges) from 10 to 20 June 2008 is shown in Fig. 10b, and Fig. 10c shows the wind data over the ZRE. One cloud-free MODIS mage of the ZRE on 20 June 2008 was found, and its derived SSC distribution is shown in Fig. 10a. Over the period 15–20 June 2008, the Zhujiang River discharge exceeded 40 000 m^3/s, with a peak discharge of up to 60 000 m^3/s. This major flood event carried a high suspended sediment load into the ZRE, which was distributed around the estuary by the combined effects of the river discharge, waves, and tides. Moreover, on 17–18 June 2008, 2 d before the MODIS image was captured, an SW wind with a maximum wind speed of approximately 14 m/s developed over the ZRE region. On 19 June 2008, an ESE with a wind speed of approximately 10 m/s blew across the estuary but on 20 June the wind direction changed and the speed fell to 3 m/s. These strong SW and ESE winds played an important role in controlling the SSC levels and sediment transport. First, the SW wind increased wave activity over the middle and eastern shoals, and the ESE wind generated larger waves over the western and northern shoals of the estuary, which resuspended more sediment from the bed into the water column and increased the SSC over most of the shoals (Fig. 10a). Under the increased river discharge, the strong SW wind changed the distribution of the ZRE plume and induced an obvious eastward flow combined with the wind-driven and buoyancy currents (Ou et al., 2009; Zu et al., 2014). Enough suspended sediment was transported into the ZRE by rivers, tides, and wind to cause the high SSC levels across almost the entire ZRE, whereas outside the estuary, the high concentrations of suspended sediment were transported eastward by the wind-driven and buoyancy currents, as shown in Fig. 10a.

4 Discussion

As in most estuaries in the world, river discharge is a very important driving force for the movement of suspended sediment. As the result of suspended sediment transport at any time in an estuary, the horizontal distribution of surface SSC at the MODIS imaging time can reflect the relative cumulative effect of the river discharge. The river discharge has very important effects on the SSC in the ZRE, especially at the seasonal scale. To quantify these variations, we calculated the area with an SSC greater than 0.01 kg/m^3 averaged over monthly and annual periods, and the results are shown in Fig. 11. In general, the area of the high SSC in the ZRE was small in spring but sharply increased in summer up to a maximum in June, when the area of the high SSC exceeded 10 000 km^2. In autumn, the SSC area greater than 0.01 kg/m^3 decreased. As was indicated in Section 2.2, 78.0% of the total Zhujiang River discharge and sediment load is carried during the flood season between April and September; approximately 50.0% of the total discharge runs into the ZRE in summer (June–August), whereas only approximately 10.0% runs into the ZRE in winter. The combination of seasonal runoff and tidal currents transport the suspended upstream sediments through the eight outlets and into the surrounding estuary. The higher the Zhujiang River discharge, the more the sediment discharged into the estuary and the higher the SSC in the mouth and adjacent seas. From 2002 to 2012, the total monthly averaged river discharge at the Gaoyao and Shijiao Stations followed similar annual cycles, with elevated SSC levels (>0.1 kg/m^3) covering the area shown in Fig. 12. The highest river discharge occurs in summer, and the highest SSC levels and the largest area of the high SSC levels occurs in the

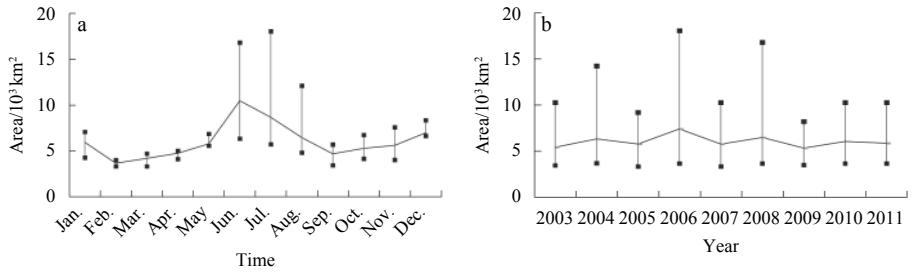

Fig. 11. Seasonal and interannual variations in the areas of the ZRE covered by (MODIS-derived) SSCs greater than 0.01 kg/m³ from 2003 to 2011 (solid black line) and minimum and maximum monthly values over this period.

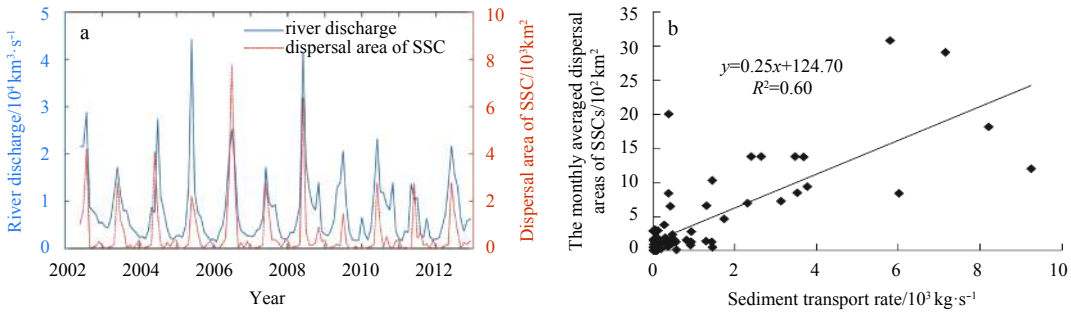

Fig. 12. Time series of monthly averaged discharges at the Gaoyao and Shijiao stations and monthly averaged dispersal areas of MODIS-measured SSC greater than 0.1 kg/m³ across the ZRE from 2002 to 2012 (a), and linear correlation between the monthly averaged dispersal areas of SSCs greater than 0.1 kg/m³ and the monthly averaged sediment transport rate of the Zhujiang River (b).

ZRE. There is a linear correlation between the monthly suspended sediment discharge and the dispersal area, with a correlation coefficient of 0.58. The suspended sediment load of the Zhujiang River discharged into the estuary had greater correlation to the SSC in the estuary and the high SSC dispersal area, which resulted in the SSCs that were higher in summer and lower in spring and autumn. The linear correlation coefficient of the monthly averaged sediment load and the higher SSC (>0.1 kg/m³) dispersal area was 0.6 (Fig. 12b).

The Zhujiang River discharge is the smallest in winter, but the average dispersal area of high SSC increases in winter in the study period, as shown in Fig. 11. In winter, the river discharge is not a dominant driving force, and winter monsoons become very important in controlling the resuspension and net transport of fine sediment in the ZRE. The important effect of the wind waves on the resuspension of shoal sediment in winter is typical in the west shoal, as shown in Fig. 8. Under the NE wind, the fetch over the southwestern shoals was stable, and the wind waves increased with the wind speed. With the increase in the wind speed, the wave power increased, and the amount of, and area affected by, sediment resuspension also increased. This led to the higher SSC over a wider area. As shown in Fig. 13a, the area covered by SSC greater than 0.05 kg/m³ has a linear relationship with the northerly wind speed. Under calm conditions (wind speed less than 4.0 m/s), the wind-induced waves are small and could not cause sediment resuspension; consequently, the area of the low SSC showed little change (Fig. 6). The least river sediment inputs in winter or spring and the small extension of the low SSC as in Case I occurred under calm weather.

In fact, the effects of the river discharge and the wind on the SSC estuary overlaid the tides. For MODIS imaging, the time interval is longer than the semidiurnal tidal period, and the resuspension and transport of fine sediment by tidal current cannot be directly observed and distinguished from the images. The sediment resuspension by the ebb and flood currents in the Lingding Bay and Huangmao Bay has been reported in previous studies (Gong et al., 2014; Zhang et al., 2010). These studies show that the ebb current is larger than the flood current, and the SSC in the deeper outer estuary is lower than that in the upper estuary. Under the constraint of the Lingding and Huangmao Bays estuarine

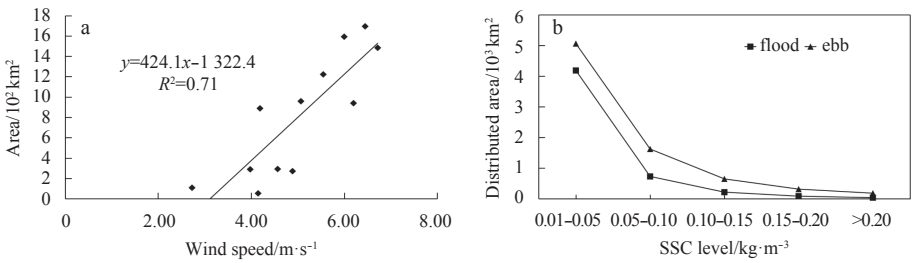

Fig. 13. The relationship between the dispersal areas of SSCs greater than 0.05 kg/m³ and the northerly wind speed (a) and differences in SSC levels during flood and ebb tides (b).

topography, the tidal flood current flows north into the estuary, and the maximum observed flood velocity exceeds 1.0 m/s, whereas the ebb current flows south with a maximum velocity greater than 1.5 m/s (Gong et al., 2014; Mao et al., 2004). From the suspended advection by the flood and ebb currents, the flood current carries water offshore with a lower SSC than that flowing north into the upper estuary and inhibits the outwards diffusion of the higher-SSC water from the nearshore areas, but the ebb current accelerates the dispersal of the higher SSC. In this study, we simulated the tidal levels between 2002 and 2012 across the ZRE using the Oregon State University Tidal prediction Software. The imaging times of the 108 MODIS images and tidal level series from the ZRE were then compared to determine the advection effect of the flood and ebb tides on the spatial distribution of elevated SSC levels. The areas covered by the five SSC criteria defined using the above concentrations were calculated for the 108 images and averaged for the flood and ebb tides. The results show that the mean areas covered by the five SSC criteria are less under flood tides than under ebb tides (Fig. 13b). This means that the flood current causes the areas of higher SSC levels to decrease, and the ebb current increases the southerly, southwesterly or southeasterly dispersal and extension of the higher SSCs in the nearshore zone.

5 Conclusions

Because the ZRE is in a region of frequent cloud cover and rain, the number of high-quality MODIS images of the ZRE captured each year is relatively low, with most images coming from the winter and the fewest from the spring. In this study, 108 cloud-free MODIS images of the ZRE over the period 2002-2012 were selected to study the temporal and spatial changes in the SSC. On the basis of the empirical exponential retrieval model we developed in previous studies, 108 MODIS-derived SSC distributions were computed. In addition, the corresponding Zhujiang River discharges, the winds over the ZRE, and the tides at the Lingding Bay mouth were statistically considered to estimate the effects of these factors on SSC dispersal and variation. Under varied runoff and wind conditions, five different dynamic and dominant SSC dispersal patterns were outlined for the ZRE. Under very low discharge in the dry season and a weak wind, Case I shows the low SSCs in the estuary. A huge Zhujiang river discharge in Case II controlled the dispersal of the suspended sediment and transport from the outlets and formed the river-dominant dispersal pattern of the high SSCs. Case III shows the wind-dominant dispersal of the high SSCs derived from the west shoal and southwesterly transport under a strong NE wind. Case IV is the combination of relatively large runoff and wind. Case V is caused by a strong tropical storm with high river discharge and wind, which is characterized by the high SSCs across the entire estuary that were transported eastward by the wind-driven and buoyancy currents outside the estuary.

At a seasonal scale, runoff is the dominant cause of the SSC variations in the ZRE. The area of the high SSC levels is largest in summer, with correlation coefficients between monthly averaged river discharge and the area covered by the high SSCs of approximately 0.6. The suspended sediment loads supplied by the eight outlets differed; thirty-six percent of the Zhujiang River suspended sediment load discharged into the Modaomen Bay and another 40% of the Zhujiang River discharge and the suspended sediment load went through the Hengmen, Hongqimen, and Jiaomen Bays and onto the west shoal of the Lingding Bay mouths, which caused the SSC levels in these areas to be greater than over the other shoals near the outlets into the estuary. The northeastern monsoon is the dominant cause of sediment resuspension over the western shoals of the ZRE; it transports this material southwestward to form the dispersal pattern of Case III. The area of elevated SSCs was linearly correlated with the northerly wind speed, with a coefficient of up to 0.7. The effect of the river discharge and the wind on the SSC overlapped the tides, and the advection effect of the tidal current caused the SSC areas greater than 0.05 kg/m^3 to be larger on the ebb tides than the flood tides.

Acknowledgements

We are thankful to colleagues and faculty members in the Institute of Estuarine and Coastal Research who have provided many suggestions and great assistants in the sampling data.

References

Alvarez, Gomez-Gesteira M, Decastro M, et al. 2014. Comparison of different wind products and buoy wind data with seasonality and interannual climate variability in the southern Bay of Biscay (2000-2009). Deep-Sea Research Part II-Topical Studies in Oceanography, 106: 38–48, doi: 10.1016/j.dsr2.2013.09.028

Bourrin F, Friend P L, Amos C L, et al. 2008. Sediment dispersal from a typical Mediterranean flood: The Têt River, Gulf of Lions. Continental Shelf Research, 28(15): 1895–1910, doi: 10.1016/j.csr.2008.06.005

Chen Shuisen, Huang Wenrui, Chen Weiqi, et al. 2011. Remote sensing analysis of rainstorm effects on sediment concentrations in Apalachicola Bay, USA. Ecological Informatics, 6(2): 147–155, doi: 10.1016/j.ecoinf.2010.12.001

Chen Shuisen, Huang Wenrui, Wang Hongqing, et al. 2012. Remote sensing assessment of sediment re-suspension during Hurricane Frances in Apalachicola Bay, USA. Remote Sensing of Environment, 113(12): 2670–2681

Chen Weibo, Liu Wencheng, Hsu M H, et al. 2015. Modeling investigation of suspended sediment transport in a tidal estuary using a three-dimensional model. Applied Mathematical Modelling, 39(9): 2570–2586, doi: 10.1016/j.apm.2014.11.006

Cuvilliez A, Lafite R, Deloffre J, et al. 2015. River flow control on intertidal mudflat sedimentation in the mouth of a macrotidal estuary. Geomorphology, 239: 174–181, doi: 10.1016/j.geomorph.2015.03.020

Doxaran D, Froidefond J M, Castaing P, et al. 2012. Dynamics of the turbidity maximum zone in a macrotidal estuary (the Gironde, France): Observations from field and MODIS satellite data. Estuarine, Coastal and Shelf Science, 81(3): 321–332

Fagherazzi S, Mariotti G, Banks A T, et al. 2014. The relationships among hydrodynamics, sediment distribution, and chlorophyll in a mesotidal estuary. Estuarine, Coastal and Shelf Science, 144: 54–64, doi: 10.1016/j.ecss.2014.04.003

Feng Lian, Hu Chuanmin, Chen Xiaoling, et al. 2014. Influence of the Three Gorges Dam on total suspended matters in the Yangtze Estuary and its adjacent coastal waters: Observations from MODIS. Remote Sensing of Environment, 140: 779–788, doi: 10.1016/j.rse.2013.10.002

Fernández-Nóvoa D, Mendes R, deCastro M, et al. 2015. Analysis of the influence of river discharge and wind on the Ebro turbid plume using MODIS-Aqua and MODIS-Terra data. Journal of Marine Systems, 142: 40–46, doi: 10.1016/j.jmarsys.2014.09.009

Freeman Freeman A M, Jose F, Roberts H H, et al. 2015. Storm induced hydrodynamics and sediment transport in a coastal Louisiana lake. Estuarine, Coastal and Shelf Science, 161: 65–75, doi: 10.1016/j.ecss.2015.04.011

Gong Wenping, Jia Liangwen, Shen Jian, et al. 2014. Sediment transport in response to changes in river discharge and tidal mixing in a funnel-shaped micro-tidal estuary. Continental Shelf Research, 76: 89–107, doi: 10.1016/j.csr.2014.01.006

Gong Wenping, Shen Jian. 2012. Response of sediment dynamics in the York River Estuary, USA to tropical cyclone Isabel of 2003. Estuarine, Coastal and Shelf Science, 84(1): 61–74

Green M O, Coco G. 2014. Review of wave-driven sediment resuspension and transport in estuaries. Reviews of Geophysics, 52(1): 77–117, doi: 10.1002/rog.v52.1

Lahet F, Stramski D. 2010. MODIS imagery of turbid plumes in San Diego coastal waters during rainstorm events. Remote Sensing of Environment, 114(2): 332–344, doi: 10.1016/j.rse.2009.09.017

Lawson S E, Wiberg P L, Mcglathery K J, et al. 2007. Wind-driven sediment suspension controls light availability in a shallow coastal lagoon. Estuaries and Coasts, 30(1): 102–112, doi: 10.1007/BF02782971

Li Zhanhai, Li M Z, Dai Zhijun, et al. 2015. Intratidal and neap-spring variations of suspended sediment concentrations and sediment transport processes in the North Branch of the Changjiang Estuary. Acta Oceanologica Sinica, 34(1): 137–147, doi: 10.1007/s13131-015-0605-z

Li P, Yang S L, Milliman J D, et al. 2012. Spatial, temporal, and human-induced variations in suspended sediment concentration in the surface waters of the Yangtze Estuary and adjacent coastal areas. Estuaries and Coasts, 35(5): 1316–1327, doi: 10.1007/s12237-012-9523-x

Lihan T, Saitoh S I, Iida T. 2008. Satellite-measured temporal and spatial variability of the Tokachi River plume. Estuarine, Coastal and Shelf Science, 78(2): 237–249, doi: 10.1016/j.ecss.2007.12.001

Liu Xiaohai, Huang Wenrui. 2012. Modeling sediment resuspension and transport induced by storm wind in Apalachicola Bay, USA. Environmental Modelling & Software, 24(11): 1302–1313

Liu Xiaoming, Wang Menghua. 2014. River runoff effect on the suspended sediment property in the upper Chesapeake Bay using MODIS observations and ROMS simulations. Journal of Geophysical Research: Oceans, 119(12): 8646–8661, doi: 10.1002/2014JC010081

Mao Q W, Shi P, Yin K D, et al. 2004. Tides and tidal currents in the Pearl River Estuary. Continental Shelf Research, 24: 1797–1808, doi: 10.1016/j.csr.2004.06.008

Moreira D, Simionato C G, Gohin F, et al. 2013. Suspended matter mean distribution and seasonal cycle in the Río de La Plata estuary and the adjacent shelf from ocean color satellite (MODIS) and in-situ observations. Continental Shelf Research, 68: 51–66, doi: 10.1016/j.csr.2013.08.015

Nezlin N P, DiGiacomo P M, Diehl D W, et al. 2008. Stormwater plume detection by MODIS imagery in the southern California coastal ocean. Estuarine, Coastal and Shelf Science, 80(1): 141–152, doi: 10.1016/j.ecss.2008.07.012

Ou Suying, Zhang Hong, Wang Dongxiao. 2009. Dynamics of the buoyant plume off the Pearl River Estuary in summer. Environmental Fluid Mechanics, 9(5): 471–492, doi: 10.1007/s10652-009-9146-3

Percuoco V P, Kalnejais L H, Officer L V. 2015. Nutrient release from the sediments of the Great Bay Estuary, N. H. USA. Estuarine, Coastal and Shelf Science, 161: 76–87, doi: 10.1016/j.ecss.2015.04.006

Petus C, Chust G, Gohin F, et al. 2010. Estimating turbidity and total suspended matter in the Adour River plume (South Bay of Biscay) using MODIS 250-m imagery. Continental Shelf Research, 30(5): 379–392, doi: 10.1016/j.csr.2009.12.007

Petus C, Marieu V, Novoa S, et al. 2014. Monitoring spatio-temporal variability of the Adour River turbid plume (Bay of Biscay, France) with MODIS 250-m imagery. Continental Shelf Research, 74: 35–49, doi: 10.1016/j.csr.2013.11.011

Wu Guofeng, Liu Liangjie, Chen Fangyuan, et al. 2014. Developing MODIS-based retrieval models of suspended particulate matter concentration in Dongting Lake, China. International Journal of Applied Earth Observation and Geoinformation, 32: 46–53, doi: 10.1016/j.jag.2014.03.025

Xing Qianguo, Lou Mingjing, Chen Chuqun, et al. 2013. Using in situ and satellite hyperspectral data to estimate the surface suspended sediments concentrations in the Pearl River Estuary. IEEE Journal of Selected Topics in Applied Earth Observations and Remote Sensing, 6(2): 731–738, doi: 10.1109/JSTARS.2013.2238659

Yang Ganran, Chen Lianggui. 1987. Wave characteristics and calculation of typhoon wave in Mawan harbour. Tropic Oceanology (in Chinese), 6(1): 66–72

Zhang Wei, Xu Zheng, Dong Xue, et al. 2010. Analysis on characteristics of temporal and spatial variation of suspended sediment in the Lingding Bay. Journal of Sediment Research (in Chinese), (4): 22–28

Zu Tingting, Wang Dongxiao, Gan Jianping, et al. 2014. On the role of wind and tide in generating variability of Pearl River plume during summer in a coupled wide estuary and shelf system. Journal of Marine Systems, 136: 65–79, doi: 10.1016/j.jmarsys.2014.03.005